THE ASTROPHYSICAL JOURNAL, 459:671–685, 1996 March 10

EQUATORIAL WIND COMPRESSION EFFECTS ACROSS THE H-R DIAGRAM

R. IGNACE,[1] J. P. CASSINELLI, AND J. E. BJORKMAN
Department of Astronomy, University of Wisconsin, 5534 Sterling Hall, 475 N. Charter Street, Madison, WI 53706-1582
Received 1995 June 5; accepted 1995 September 15

ABSTRACT

We investigate the degree to which moderate stellar rotation rates can influence the two-dimensional density structure in the winds of four classes of stars: Wolf-Rayet, B[e], asymptotic giant branch (AGB), and novae. These classes are distributed across the H-R diagram and have a wide range of escape speeds and wind acceleration. Furthermore, all have members which possess asymmetric circumstellar nebulae. It has been suggested that these asymmetries could result from stellar winds which have moderate equatorial density enhancements. Large enhancements may arise as the result of stellar rotation as demonstrated by the wind-compressed disk (WCD) model of Bjorkman & Cassinelli. Instead of a dense disk, here we consider a milder distortion called a wind-compressed zone (WCZ). A WCZ is said to occur if a star rotates more slowly than the disk formation threshold and if the density at the equator is more than about 3 times that at the pole. We assume that the stellar winds obey a standard β-velocity law and consider the effects of varying two of the velocity law parameters: the terminal speed, v_∞, and the exponent, β. For a given rotation rate, the wind compression is enhanced as either v_∞ is decreased or β is increased, because both correspond to a smaller acceleration of the wind. A general result from our model simulations is that the asymptotic density and flow structure are predominantly governed by the ratio ω/ω_D, where ω is the stellar rotation rate normalized to the critical speed and ω_D is the threshold value needed for disk formation. For the Wolf-Rayet and B[e] models which have moderate wind terminal speeds and shallow velocity laws ($\beta = 3$), a WCZ can form even at rotation rates of order 10% and 20% critical, respectively. For the AGB model with a low terminal speed and a $\beta = 3$ velocity law, a WCZ can form at 15% critical. Finally, we consider novae, which have time-variable wind properties. In particular, the location of the sonic point is time dependent, so we compute models with a range of sonic point radii. In favorable cases, a WCZ can form for white dwarf rotation rates of less than 20% critical; however, further work will be required to properly treat the extended subsonic region of nova winds.

Subject headings: novae, cataclysmic variables — stars: AGB and post-AGB — stars: mass loss — stars: rotation — stars: Wolf-Rayet

1. INTRODUCTION

With astrophysical observations of better resolution, it is becoming apparent that aspherical mass loss occurs for stars throughout the H-R diagram. Perhaps one of the most striking examples of a bipolar flow comes from *Hubble Space Telescope* images that reveal a strong axisymmetric geometry for the circumstellar envelope of the luminous blue variable (LBV), η Carinae (Ebbetts et al. 1992; Hester et al. 1995). Other LBV stars also have axisymmetric nebulae, such as AG Car (Leitherer et al. 1994; Schulte-Ladbeck et al. 1994) and HR Car (Hutsemékers & Van Drom 1991; Schulte-Ladbeck et al. 1993a). Some other hot stars exhibiting aspherical mass loss include the Be stars, the B[e] stars, and the Wolf-Rayet stars. The Be and B[e] winds are thought to harbor dense equatorial disks, as evidenced by their infrared excess, line profile shapes, and polarimetric properties (Coté & Waters 1987; Struve 1931; Coyne & McLean 1982; Allen & Glass 1976; Zickgraf et al. 1985; Schulte-Ladbeck et al. 1992). Among the Wolf-Rayet stars, some exhibit intrinsic polarization, and aspherical ring nebulae are observed in a few cases (Schulte-Ladbeck et al. 1991; Schulte-Ladbeck, Hillier, & Nordsieck 1993b; Nota et al. 1995).

Aspherical wind phenomena also have relevance for the outflows of cool giant and supergiant stars. It has been suggested that the SN 1987A ring could result from the expansion of the supernova explosion into an equatorially enhanced slow wind from the red supergiant phase (Luo & McCray 1991; Wang & Mazzali 1992; Blondin & Lundqvist 1993). Although not as explosive, a similar scenario may account for the broad range of observed planetary nebula (PN) morphologies (Balick 1987; Kahn & West 1985; Icke 1988). In PNe, the fast low-density wind from the central star of the PN overtakes the slow, dense aspherical wind driven off the star during the asymptotic giant branch (AGB) phase. The resulting wind-wind collision generates a thin, dense expanding shell and a bipolar nebula (Frank & Mellema 1994). As one last example, the expanding shells from many nova outbursts are also observed to be aspherical and often axisymmetric with elliptical or bipolar morphologies (Rosino 1977; Duerbeck 1987).

In all of these examples, there are two ways in which the wind geometries are distorted: (1) the mass loss from the star is aspherical and/or (2) the outflow becomes aspherical after leaving the star. There are several mechanisms for generating an aspherical mass loss of the first kind. If a star is rotating rapidly, additional material may be ejected from the equatorial region as a result of the reduced gravity (Friend & Abbott 1986). An example is the rotationally induced bi-stability mechanism of Lamers & Pauldrach (1991). If the wind near the equator becomes optically thick in the Lyman continuum, a change in the distribution of lines that drive the wind will result, such that the equatorial mass loss increases dramatically and the flow becomes slower and denser than the polar wind. Rapid stellar

[1] rico@astro.wisc.edu.

rotations may occur in some single stars as a result of star formation, or in binary systems as a result of "spin-up" from the secondary (Livio & Soker 1988). In addition to rotation, magnetic effects can also lead to equatorially enhanced wind flows (Hartmann & MacGregor 1982; Poe, Friend, & Cassinelli 1989).

For aspherical mass loss of the second kind, some distortion and density enhancement is produced in the wind itself. Bjorkman & Cassinelli (1993, hereafter BC) developed a wind compression model for rotating stars, in which angular momentum conservation leads to an equatorially enhanced wind density. For a star that is part of a binary, the companion object can gravitationally focus the wind from the primary so that a wind enhancement forms in the secondary's orbital plane (Friend & Castor 1982). Finally, if a toroidal magnetic field exists in the wind, magnetic tension in the equatorial region can "pinch" the flow at a shock interface, resulting in an axisymmetric wind bubble that is extended along the poles (Chevalier & Luo 1994).

In this paper we concentrate on the rotational distortion effects that occur in the wind (intrinsic or arising from spin-up). The effects of rotation on winds have become better understood through the consideration of two-dimensional flow effects by BC and Owocki, Cranmer, & Blondin (1994). These papers developed the wind-compressed disk (WCD) model for an axisymmetric isothermal line-driven wind. Results were presented for Be stars, for which there is clear spectral evidence of rapid rotation. In the wind compression model, flow from higher latitudes orbits toward the equator. The depletion of stellar wind material from higher latitudes results in a density enhancement at the equator. If the component of the flow speed perpendicular to the equator is supersonic, then a pair of shocks form above and below an equatorial disk. The postshock cooling creates a very dense *disk* (i.e., a WCD). In the WCD models, typical $v \sin i$ rotation rates of Be stars, which range from 30% to 80% critical, are sufficient to form high-density, shock-compressed equatorial disks. It is essential that the wind compression produce a shock-bounded disk for there to be a 2–3 order of magnitude increase in the density that is necessary to explain many of the observations. These include strong Balmer emission lines, IR continuum excesses, and intrinsic polarization.

In addition to Be stars, the winds from other stellar types may also be affected by equatorial wind compression. Although the wind compression model of BC was originally developed in the context of line-driven winds, the expressions governing the wind flow are kinematical and do not require the wind to be line driven. So, independent of the wind-driving mechanism, if the velocity distributions used in the wind model are a good approximation to the outflow of a star, and if all other model assumptions (discussed in the following section) are fulfilled, then the wind compression model should yield the correct stellar wind structure.

In developing the WCD model, it was found that disk formation becomes more likely if (1) the star is rotating more rapidly or (2) the wind acceleration is small, in which case disk formation can occur at rotation rates that are slow relative to breakup. The radial acceleration of a steady state wind is $v_r(dv_r/dr)$, and it follows that the wind acceleration will be small if the wind terminal speed, v_∞, is small (since $v_r \leq v_\infty$) or the velocity gradient, dv_r/dr, of the wind is small. Thus, stellar winds that are most likely to be affected by wind compression are those with low terminal speeds or small velocity gradients.

In the case of the rotating Be stars, their winds are affected by wind compression because they have relatively small terminal speeds. The presence of a thin, dense disk is suggested by line emission observations from the Be winds. However, in the stellar winds of many other types of stars, *disks* are not always necessary to explain the observations, such as the polarization of Wolf-Rayet winds or the elliptical morphologies of PNe. So in this paper we emphasize wind-compressional effects in the regime of slow rotations, where there is a significant equatorial density enhancement but a shock-compressed disk does not form. We refer to these models without disks as "wind-compressed zone" (WCZ) models.

The primary purpose of this paper is to assess the occurrence of wind-compressional effects across the H-R diagram. Threshold rotation rates for a sequence of equatorial compressions are determined for the winds of several different stars. This paper is structured as follows. In § 2 the formulae describing the wind flow structure and density distribution of the WCZ model are presented. The consequences of the wind acceleration for the rotational distortion of the wind are examined in § 3. In § 4 we compute the wind structure for a WN5 star, a B[e] star, an AGB star, and a nova white dwarf, and the results are discussed for each individual object. A summary is given in § 5. Appendices A and B detail derivations of the WCZ streamline trajectories and the wind density distribution, respectively.

2. THE WIND-COMPRESSED ZONE MODEL

We divide this section into three parts. In the first part, the rotating wind model is introduced, wherein the model assumptions are described and the model parameters are defined. In the second part, the streamline trajectories for the wind flow are discussed, and in the last segment, the wind density structure is developed.

2.1. *The Rotating Wind Model*

In a steady state rotating isothermal stellar wind with a density, ρ, and velocity, $\boldsymbol{v}$, the conservation of momentum can be expressed as

$$\rho(\boldsymbol{v} \cdot \nabla)\boldsymbol{v} = -v_s^2 \nabla\rho + \rho \boldsymbol{f}, \tag{1}$$

where v_s is the isothermal speed of sound and $\boldsymbol{f}$ is the net external force per unit mass, including gravitation and radiative acceleration. BC consider the supersonic portion of this wind and argue that the gas pressure gradient force will be negligible if the stellar rotation and wind terminal speed are larger than the isothermal speed of sound. After dropping the pressure gradient force, the remaining forces are central forces that do not exert torques on the flow, so the total angular momentum is conserved along streamlines. An analytic solution for the wind structure follows because the motion of individual fluid elements will be confined to a plane.

Figure 1 illustrates three trajectories that a fluid element of the supersonic wind might follow. Consider a fluid element that is injected into the supersonic wind at a release point, r_0, near the surface of the rotating star at an initial co-latitude, θ_0. Because the forces are radial, this fluid element travels in a plane that passes through the center of the star (designated as the "orbital plane") and is inclined with respect to the equatorial plane. For case (*a*), the outward radial forces are so large as to cause the flow to quickly develop a nearly radial trajectory. Case (*a*) represents the outflow in most rotating O star winds. For case

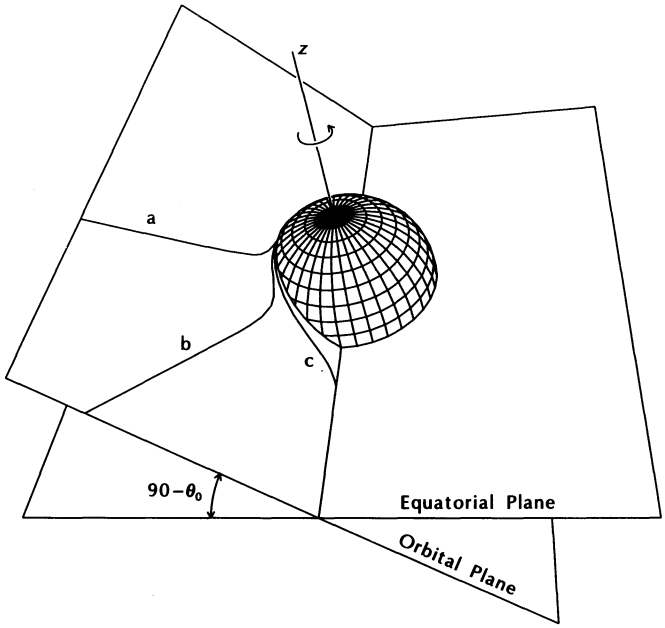

FIG. 1.—Trajectories in the orbital plane for a streamline originating at polar angle θ_0. The trajectory labeled (*a*) is for a slow rotator and/or a large wind acceleration. There is little tendency for the flow to form a significant equatorial wind compression in this case. The trajectory labeled (*b*) is one that would occur in a star with a moderate rotation rate and a slowly accelerating wind. Conditions that lead to a preponderance of this type of streamline also lead to a significant equatorial compression of the wind. The trajectory labeled (*c*) results for a rapidly rotating star and a large wind acceleration or for a star with a more moderate stellar rotation and a small wind acceleration. In this case, a dense shock-bounded disk forms in the equatorial region.

(*c*), the force of gravity dominates the flow in the region close to the star, so the trajectory tends to bend around the star, and material orbits downward to the equator. If the trajectory crosses the equatorial plane, a WCD forms. Case (*c*) thus represents the flow occurring in Be star winds. Case (*b*) is an intermediate case in which a streamline experiences some deflection toward the equator, but a WCD does not develop. Nevertheless, the wind becomes aspherical, having a significant equatorial density enhancement (i.e., a WCZ). The development of case (*b*) is of primary interest in this paper.

To obtain a quantitative description of the equatorial wind compression, BC adopted functions for the velocity distribution that fit the numerical solution of Friend & Abbott (1986) for the one-dimensional equatorial wind problem. These fitted velocity functions were extended to two dimensions, providing a kinematical description of the fluid element motions in the orbital plane. We present a modified set of kinematical relations from which we derive a new wind model. The four equations governing the wind flow of our model are

$$v'_r(r', \theta_0) = v_0 + [v_\infty(\theta_0) - v_0]\left(1 - \frac{r_0}{r'}\right)^\beta , \quad (2)$$

$$v_\infty(\theta_0) = \zeta v_{\rm esc}\left(1 - \sin\theta_0 \frac{v_{\rm rot}}{v_{\rm crit}}\right)^\gamma , \quad (3)$$

$$v'_\phi(r', \theta_0) = v_{\rm rot} \sin\theta_0 \left(\frac{r_0}{r'}\right) , \quad (4)$$

$$\dot{M}(r_0, \theta_0) = \dot{M}_0 . \quad (5)$$

The primes denote quantities measured in the orbital plane (using spherical coordinates). Equation (2) is the β-velocity law that we use to describe the radial component of the wind flow velocity, v'_r. The radius r_0 is the release point (i.e., the location beyond which the pressure gradient forces may be ignored), and v_0 is the radial speed at that point. We take r_0 to be the sonic radius, r_s, which, except for our nova model, we assume is near the stellar surface (assumed to be spherical with radius R_*). Since r_0 is set equal to the sonic point radius, we have $v_0 = v_s$. The velocity exponent, β, controls the radial extent of the wind acceleration, with larger values of β producing shallower velocity laws at the base of the wind. Thus, dv_r/dr decreases as β increases. The latitudinal dependence of the radial velocity enters through the terminal speed. As is seen in equation (3), the wind terminal is assumed to scale as the stellar escape speed, $v_{\rm esc}$, times a constant of proportionality, ζ. The escape speed is $v_{\rm esc} = [2GM_*(1 - \Gamma)/R_*]^{1/2}$, where Γ is the ratio of radiative to gravitational acceleration. The exponent γ determines the ratio of the equatorial to polar wind terminal speeds. Larger values of γ imply a greater sensitivity of the terminal speed to the rotation speed. Based on the results of Friend & Abbott (1986), BC used a value of $\gamma = 0.35$. The azimuthal component of the velocity in the orbital plane, v'_ϕ, is determined by conservation of angular momentum and is given in equation (4). Appearing in equation (5) is the mass-loss distribution at the lower boundary, which we assume to be spherically symmetric and constant.

The expressions (2)–(5) differ somewhat from those of BC (their eq. [15]). BC used a β-velocity law of the form $v'_r = v_\infty(\theta_0)(1 - R_*/r')^\beta$, for which the velocity is zero at the stellar surface. When calculating the streamline deflection, ϕ', they chose the release point at $r_0 = R_*$, since the sonic radius was so close to R_* (with $r_s \approx 1.01R_*$). However, Owocki et al. (1994) pointed out that since BC started their integration of the ϕ' deflection at $v_r = 0$ instead of $v_r = v_s$, BC overestimated the ϕ' deflection. To obtain adequate agreement between the analytical and numerical results, Owocki et al. found that it was essential to chose the release point at $v_r = v_s$, the location at which the gas pressure support becomes negligible.

It is generally assumed that the gas pressure support is lost when each component of the flow velocity attains a value of order the sound speed. For O and B star winds, the transonic zone is typically narrow, so choosing $r_0 = r_s$ produces excellent agreement with the results of Owocki et al. However, when the transonic zone becomes radially extended (as will be the case for large β-values), it becomes less clear where the release point actually occurs because the gas pressure support is only gradually lost with increasing radius. Since gas pressure gradients in the θ-direction will tend to resist the equatorial compression, one might expect that choosing $r_0 = r_s$ will tend to overestimate the wind distortion. Yet, the gradual loss of gas pressure support also suggests that some equatorial compression will occur *prior* to the sonic point; therefore, lacking a detailed hydrodynamical calculation, we expect that on average the sonic point is the best estimate for the release point.

Large β-values may also have implications for the subsonic zone. Setting $r_s = R_*$ implies that the subsonic flow is characterized by a small pressure scale height. However, as β increases, the transonic region becomes extended, and the pressure scale height in the vicinity of r_s becomes large, implying that the subsonic region might also be radially

extended. Whether or not the subsonic region is extended will depend on the wind-driving mechanism, but an extended subsonic region can have dramatic effects on the equatorial compression (see § 4.4 on nova winds). Consequently, our model results for $\beta > 1$ are likely to be qualitatively correct, but accurate quantitative results at large β are likely to change once radiative hydrodynamical simulations become available.

Another difference between our wind description and that of BC is that we choose the mass-loss rate to be spherically symmetric at the stellar surface, whereas the mass-loss rate used by BC is a function of θ_0 at the stellar surface. The mass-loss rate of BC has a minimum at the poles and increases toward the equator owing to the reduction in the equatorial surface gravity of rapidly rotating stars. We choose the simpler approximation because our applications here include several classes of stars for which the initial distribution of mass loss is not well known. We also prefer not to introduce a poorly known parameter to describe the mass-loss rate. Nevertheless, it is clear that the mass-loss distribution of BC (with mass loss increasing toward the equator) tends to *increase* the equatorial density relative to the spherical case, so in this regard our results for the equator to pole wind density contrast will be lower limits.

2.2. *The WCZ Wind Structure*

For our kinematic model, the wind structure is determined by the streamline locations. The streamlines are derived from the velocity equations by taking the ratio of v'_ϕ to v'_r from equations (4) and (2). This ratio yields a first-order differential equation for the trajectory of a fluid element in the orbital plane. An expression describing this trajectory is derived in Appendix A, from which we take the result that the deflection (in the orbital plane) of a streamline from the radial direction is given by

$$\phi'(r, \theta_0) = \frac{v_{\rm rot} \sin \theta_0}{\beta v_s} \left[\frac{v_s}{v_\infty(\theta_0) - v_s} \right]^{1/\beta} B_y\left(\frac{1}{\beta}, 1 - \frac{1}{\beta}\right). \quad (6)$$

The function B_y is the incomplete Beta function (see Abramowicz & Stegun 1972) defined by an integral with a lower limit of zero and an upper limit of $y = 1 - v_s/v_r$ (see Appendix A).

At large radii, ϕ' will approach an asymptotic value, $\phi'_{\rm max}$, that is the maximal deflection experienced by a streamline originating at θ_0. Referring to Figure 1, we make the following associations: if $\phi'_{\rm max}(\theta_0)$ is small, the fluid element will deviate little from a radial trajectory, so that the wind is essentially spherical (trajectory [*a*]). As $\phi'_{\rm max}(\theta_0)$ is increased, say because the star is rotating more rapidly, the flow will orbit toward the equator, and a greater density compression results (trajectory [*b*]). If $\phi'_{\rm max}(\theta_0)$ becomes greater than $\pi/2$, the fluid element will attempt to cross the equatorial plane (trajectory [*c*]), which causes the material to enter a shock-bounded disk.

2.3. *The Wind Density Structure*

In addition to the flow geometry, the streamlines also determine the wind density distribution. To derive the wind density, ρ, it is convenient to consider streamtubes, which are funnels whose walls are determined by the streamlines. Since the streamlines cannot cross, material in a given streamtube will remain in that streamtube throughout the wind. The separation of the streamlines determines the cross-sectional area of a streamtube. For a spherical wind, the streamtube area varies with radius as $dS_{\rm sph} = dS_* r^2/R_*^2$, where dS_* is the streamtube cross section at the stellar surface. For our rotating wind model, the streamtube cross section dS is related to the spherical case by

$$dS = dS_{\rm sph}\left(\frac{d\mu}{d\mu_0}\right), \quad (7)$$

where $\mu = \cos\theta$, $\mu_0 = \cos\theta_0$, and $d\mu/d\mu_0$ is the wind compression factor which describes the expansion or contraction of the streamtube area as a function of latitude and radius. The complete expression for $d\mu/d\mu_0$ is derived in Appendix B. If the differential cross section of the streamtube grows with radial distance more gradually than r^2, the density in the tube will be enhanced relative to a spherical flow, and vice versa.

The wind density is derived from the conservation of mass within a streamtube. Beginning with the equation of mass continuity, $\nabla \cdot (\rho \boldsymbol{v}) = 0$, a surface integral over the streamtube can be obtained by an application of the divergence theorem. Using equation (7) and the condition of confinement of material in a streamtube, we find that

$$\rho = \frac{\dot{M}_0}{4\pi r^2 v_r(r, \theta_0)} \left(\frac{d\mu}{d\mu_0}\right)^{-1}. \quad (8)$$

Now let us compare the wind density from a rotating star to that of a spherical flow. For a spherical wind, the mass continuity equation gives

$$\rho_{\rm sph} = \frac{\dot{M}_0}{4\pi r^2 v_{\rm sph}(r)}. \quad (9)$$

The wind speed in the spherical case, $v_{\rm sph}$, is equal to the polar wind speed, v_p, of the rotating case, because the radial flow speed at the pole is unaffected by the stellar rotation. Combining equations (8) and (9), the density of a wind from a rotating star can be expressed as

$$\rho(r, \theta_0) = \frac{v_{\rm sph}(r)}{v_r(r, \theta_0)} \left(\frac{d\mu}{d\mu_0}\right)^{-1} \rho_{\rm sph}(r). \quad (10)$$

Let us consider the limits of equation (10) at the pole ($\theta_0 = 0$) and the equator ($\theta_0 = \pi/2$). At the pole the wind compression factor, $d\mu/d\mu_0$, reduces to $1 + [\phi'(r, 0)/x_0]^2$, where $x_0 = \sin\theta_0$ (Cranmer & Owocki 1995). Note that $\lim_{x_0 \to 0} \phi'(r, 0)/x_0$ is finite and that the polar density is smaller in a rotating wind than a spherical wind. At the equator, $d\mu/d\mu_0 = \cos\phi'(r, \pi/2)$, which is less than 1 for $\phi' < \pi/2$, so the equatorial wind density of a rotating star is larger than that of the nonrotating case by the factor, $(v_p/v_{\rm eq})(d\mu/d\mu_0)^{-1}$, where $v_{\rm eq} = v_r(r, \pi/2)$. Thus, the consequence of stellar rotation is to deplete the polar region of wind material by redirecting it toward the equator. If $\phi'(r, \pi/2)$ approaches the value of $\pi/2$, the density will become infinite at the equatorial plane because $d\mu/d\mu_0 \to 0$, so the WCZ model breaks down as streamlines attempt to cross over from one hemisphere to the other. In this limit, a WCD and its associated shocks will form.

To quantify the wind compression, we introduce the equatorial to polar density ratio, η_c, that is valid for stellar rotation rates below the disk threshold. Using densities at the pole and equator as discussed in regard to equation

(10), the density contrast is

$$\eta_c(r) = \frac{\rho_{eq}}{\rho_p} = \frac{v_p}{v_{eq}} \left\{ \frac{1 + [\phi'(r, 0)/x_0]^2}{\cos \phi'(r, \pi/2)} \right\}. \quad (11)$$

If a disk does form, a density contrast of order 10^2–10^3 is produced by shocks. The parameter η_c provides an indication of how much wind material is redistributed in latitude for the wind from a rotating star.

To summarize, we have assumed a kinematic description of the wind velocity structure and have derived expressions for the two-dimensional density distribution in the rotating wind. An equatorial density enhancement results from three effects. First, the rotation leads to a slower equatorial outflow which increases the density in proportion to v_{sph}/v_{eq}. Second, rotation affects the cross section of streamtubes through the wind and, consequently, the density of material in these streamtubes. Since the streamlines are deflected toward the equator, the wind density is decreased in the polar regions and increased near the equator. Third, the rotation will likely lead to an equatorially enhanced mass loss from the stellar surface. By adopting an initial mass-loss rate with a spherical distribution, our model results tend to give lower limits of the wind density contrast, to the extent that our assumptions regarding the release point location are correct.

3. INFLUENCE OF THE WIND ACCELERATION ON THE WIND COMPRESSION

It was demonstrated by BC that for a given radial wind acceleration (i.e., a fixed value of β), the deflection is sensitive to the scale of the terminal speed, ζ (eq. [3]). Although BC pointed out that larger values of β will result in increasingly greater wind compressions, they did not study how changes in β will affect the wind flow and density structure. Here we find that the slope of the velocity law has a dramatic influence on deflecting the streamlines away from radial trajectories.

In Figure 2 the radial velocity distribution is plotted as a function of R_*/r for different values of the velocity exponent, β. The velocity is normalized to the terminal speed, and the sound speed is $v_s = 0.01 v_\infty$. The stellar surface is at the left in this figure, so the flow travels from left to right (as indicated by the arrows). Velocity laws with $\beta < 1$ are steep velocity laws that have large wind accelerations at radii near the star and rise quickly to terminal speed. In contrast, velocity laws that are shallow have large β-values, corresponding to small wind accelerations in the vicinity of the star. For a shallow law, the outward velocity remains relatively small over an extended region. This also implies that the transonic region is extended.

The $\beta = 1$ curve in Figure 2 represents a transition in the concavity of the velocity distributions. This change in concavity is attributable to a change in the velocity gradient at the base of the wind. The velocity gradient, dv_r/dr, is proportional to $(1 - R_*/r)^{\beta - 1}$. For $\beta = 1$, dv_r/dr is finite and nonzero at the stellar surface, and the radial velocity distribution is linear in R_*/r. For $\beta > 1$, the velocity gradient is zero at the stellar surface, and the velocity distribution has positive concavity. In contrast, the velocity distribution has negative concavity for $\beta < 1$ because dv_r/dr is infinite at the stellar surface. Note that the Sobolev optical depth is proportional to $(dv_r/dr)^{-1}$, so in terms of the Sobolev optical depth at the base of the wind, velocity laws with $\beta > 1$ will generally have a large number of optically thick absorption lines, whereas those with $\beta < 1$ will have a large number of optically thin ones. We speculate that optically thick winds will have $\beta > 1$ and will tend to be more sensitive to rotationally induced distortions.

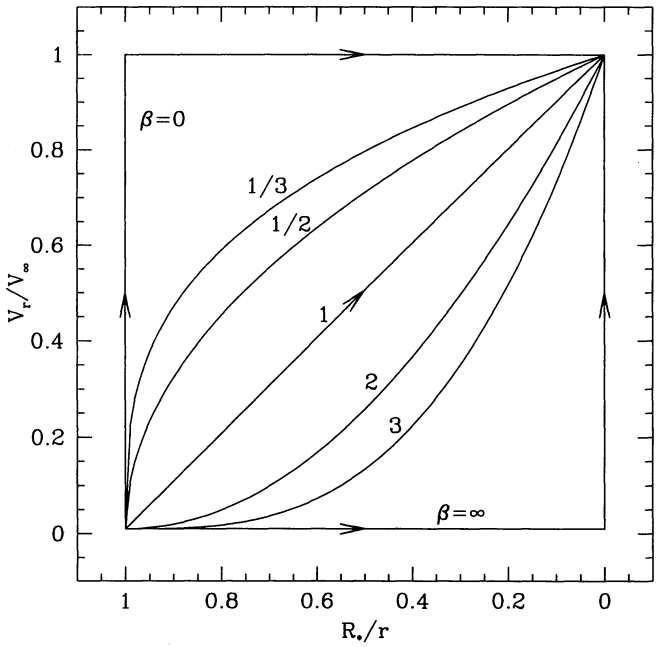

FIG. 2.—β-velocity laws normalized to the terminal speed (with $v_s = 0.01 v_\infty$) and plotted as a function of R_*/r. Seven curves are shown, each corresponding to a different β-value (as labeled). Arrows indicate that the wind flow is from left to right. The $\beta = 1$ velocity law represents a transition in the velocity gradient at $r = R_*$. Shallow velocity laws ($\beta > 1$) have $dv_r/dr = 0$ at $R_*/r = 1$, and steep velocity laws ($\beta < 1$) have $dv_r/dr \to \infty$ at $R_*/r = 1$. Note that the velocity laws with large β-values have low radial speeds of order v_s over an extended region near the star.

To understand how the slope of the velocity law affects the wind compression, we consider two asymptotic cases: a very steep velocity law (i.e., large wind acceleration) and a very shallow velocity law (i.e., small wind acceleration). These two extremes yield the maximal and minimal stellar rotation rates required to achieve disk formation for given stellar and wind parameters.

3.1. *The Limit of Very Steep Velocity Laws*

Mathematically, the steepest velocity law corresponds to the case of $\beta = 0$. Inspection of equation (2) shows that the radial velocity becomes $v_r = v_\infty(\theta_0)$ for $r > R_*$ (see Fig. 2). At this limit the acceleration to terminal speed is so large that the zone of wind acceleration is of negligible extent. Using $v_r = v_\infty$, the equation of motion in equation (A1) can be integrated to obtain the deflection

$$\phi' = \frac{v_{rot} \sin \theta_0}{v_\infty} \left(1 - \frac{R_*}{r} \right). \quad (12)$$

The deflection scales as v_{rot}/v_∞; however, from equation (3), the terminal speed also depends on the rotation speed. Consider the equatorial plane, where the deflection is maximized with respect to latitude. From equation (2) for v_∞ and equation (12) for ϕ', the maximum possible deflection is found to be

$$\phi'_{max} = \frac{1}{\sqrt{2}\zeta} \frac{\omega}{(1 - \omega)^\gamma}, \quad (13)$$

where $\omega \equiv v_{\rm rot}/v_{\rm crit}$ and ζ is the ratio of $v_\infty(\theta_0 = 0)/v_{\rm esc}$. Observed values of ζ are about 3 for O star winds (Prinja, Barlow, & Howarth 1990), as low as 1 for some B star winds (Bjorkman 1989), and 1 or less for late-type giants and supergiants (Dupree 1986). In O star winds, we expect disks to form (i.e., $\phi'_{\rm max} > \pi/2$) only for stars with rapid stellar rotations because the value of ζ is large. In contrast, for B star winds ζ is considerably smaller, so disk formation will occur at lower rotation rates. A similar result is anticipated for the winds of late-type giant and supergiant stars where, again, ζ is small.

3.2. *The Limit of Very Shallow Velocity Laws*

Shallow velocity laws are characterized by large values of β. So as an extreme case, again consider the equation of motion (A1) and allow $\beta \to \infty$. In this limit, the wind expands at a constant velocity given by the sound speed (i.e., $v_r = v_s$; see Fig. 2). The wind experiences a negligible net acceleration until the flow reaches large radii. Integration of the equation of motion gives

$$\phi' = \frac{v_{\rm rot} \sin \theta_0}{v_s}\left(1 - \frac{R_*}{r}\right). \tag{14}$$

For large values of β, the maximal deflection obtained at large radii and with $\theta_0 = \pi/2$ is

$$\phi'_{\rm max} = \frac{\omega}{\sqrt{2}}\left(\frac{v_{\rm esc}}{v_s}\right). \tag{15}$$

In contrast with equation (13), the deflection scales as $v_{\rm esc}/v_s$ instead of $\zeta^{-1} = v_{\rm esc}/v_\infty(\theta_0 = 0)$, as was the case for $\beta = 0$. Since $v_{\rm esc}/v_s$ is typically much larger than $v_{\rm esc}/v_\infty$, disk formation will occur at lower rotation speeds for stellar winds where β is large or, by extension, for any velocity law that is shallow near the base of the supersonic wind. The main effect of a shallow velocity law is to maintain a slow radial wind speed where the wind is most affected by the stellar rotation.

Although tremendously large values of the velocity exponent are not expected in stellar winds, our models indicate that the results of the large-β limit are nearly achieved even for β-values around 3 or 4. To illustrate, let us chose β to be sufficiently large that the radial velocity distribution is relatively flat from the stellar surface out to $r = 2R_*$. Let us assume further that at $r = 2R_*$, the deflection obtains 90% of $\phi'_{\rm max}$ (corresponding to some specified density contrast in the wind). If β is increased further, the radial velocity distribution becomes only slightly more flattened in the vicinity of $r = 2R_*$. In this case, 90% of the maximum deflection will still occur near $r = 2R_*$ because the radial velocity distribution is only slightly changed interior to $r = 2R_*$ (although it can significantly alter the radial velocity distribution for $r > 2R_*$). So, once β is large enough that $\phi'_{\rm max}$ is nearly attained in the region where the wind velocity distribution is relatively flat, a further increase of β will not significantly reduce the rotational threshold required to obtain a given wind density contrast.

Shallow velocity laws with $\beta > 1$ may be present in several different classes of stellar objects. Cassinelli (1991) pointed out that slowly accelerating winds may occur when the effects of multiple scattering are important. One example may be the Wolf-Rayet stars (Auer & Koenigsberger 1994; Springmann 1994; Gayley, Owocki, & Cranmer 1995; Schmutz 1995), which have massive winds. The LBV stars, which have a close evolutionary link to the Wolf-Rayet stars (see Langer et al. 1994), may be another example. Moreover, the LBV stars are often located near the Humphreys-Davidson limit, so the radiation pressure gradient greatly reduces the effective gravity of these stars, hence they may be highly susceptible to rotation, even rather slow rotation speeds. Similarly, some B supergiant stars might have slowly accelerating winds. In a spectral line profile analysis of the rapidly rotating B0.5 Ib star HD 64760, Massa, Prinja, & Fullerton (1995) find that a $\beta = 1$ velocity law produces too much scattered light at low velocities. As one possible solution, the authors suggest that the wind may be gradually accelerated at low velocities (an increase of β leads to an increase of the Sobolev optical depth and line absorption at low velocities).

3.3. *The Radial Extent of the Deflection Region*

There is one feature common to both cases of steep and shallow wind velocity laws. Equations (12) and (14) for ϕ' show that the deflection nearly reaches asymptotic values close to the star. This tendency is observed in Figure 1, which shows trajectories from model calculations. For each trajectory, most of the deflection occurs near the star, after which there is little further equatorward drift. The transition from a strong latitudinal deflection to a predominantly outward flow results from the combination of two effects. As the wind expands, the effects of rotation decrease as r^{-1}, as a result of angular momentum conservation. At the same time, the radial flow is accelerating. If the radial acceleration is large, a fluid element obtains large radii on a short timescale, so there is little equatorward deflection of the flow. Conversely, if the wind acceleration is small, the wind remains in the vicinity of the star for a relatively long time; hence, even for moderate rotation, there is ample time for an equatorial compression to form.

Since we have considered the two limiting cases of the wind acceleration, one concludes that, irrespective of the value of the velocity exponent, the wind distortion will likely take place within a few stellar radii. At larger radial distances, the wind compression is already effectively "frozen-in." This conclusion is confirmed by our model calculations, which we discuss in detail in the next section.

4. APPLICATION TO WINDS OF DIFFERENT CLASSES OF STARS

We now investigate applications of the WCZ model to members of four stellar classes: a Wolf-Rayet star, a B[e] star, an AGB star, and a white dwarf in a postnova outburst phase. These four objects were chosen because (1) they loosely span the H-R diagram in regards to escape speed and temperature, (2) there is evidence of aspherical mass loss for each of the four classes, (3) the wind acceleration in some of these objects might be small, and (4) rotation is a good candidate for producing wind distortions in all of these objects.

4.1. *Wolf-Rayet Stars*

The Wolf-Rayet (W-R) stars are massive stars with dense, fast winds, and they are generally thought to be near the terminal phase of massive star evolution prior to supernova explosion (Lamers et al. 1991). The W-R winds are most notable for the fact that the momentum of the winds exceeds that in the radiation field that is supposedly responsible for the outflow (Barlow, Smith, & Willis 1981;

Hamann, Koesterke, & Wessolowski 1993). Because of this paradox, the W-R stars have been of special interest to stellar wind theorists, and possible solutions have been discussed by Cassinelli (1991), Lucy & Abbott (1993), dos Santos, Jatenco-Pereira, & Opher (1993), Springmann (1994), and Gayley et al. (1995).

Besides having strong winds, some of the W-R stars show spectropolarimetric evidence for asymmetrical density distributions. Consequently, rotating wind models have been considered as a mechanism for producing aspherical W-R winds. Poe et al. (1989) developed a model that combined rotation, magnetic, and radiation driving forces; however, they found that rotation rates in excess of 80% critical were necessary to satisfy the density constraints imposed by radio and UV line observations. Although not in direct conflict with observations, such a high rotation rate is considered excessive and implausible from the standpoint of evolutionary considerations (Maheswaran & Cassinelli 1994).

In contrast to the equatorial expulsion model of Poe et al. (1989), the main effect of rotation in the two-dimensional WCZ model is to redirect the high-latitude wind flow toward the equatorial plane. This can lead to significant equatorial density enhancements at smaller rotation rates, especially if the wind acceleration is a gradual function of radius. We have computed the streamline geometry and the density structure expected for a typical WN5 star using the stellar parameters listed in Table 1. Although BC chose to use $\gamma = 0.35$ for their Be star wind models, we are using a value of $\gamma = 0.5$ for our W-R model because the higher value agrees better with the results of Poe's (1987) two-dimensional rotating wind model for O stars. For the other three classes of stars in this study, we use the $\gamma = 0.35$ value of BC.

The leftmost panel in Figure 3 shows W-R model results for the rotation needed to produce wind compression effects. The solid line shows, as a function of β, the threshold rotation rate to form a disk, ω_D, and the dashed lines show the rates needed to form equator to pole density contrasts by the factors indicated in the figure. As expected, the threshold rotation rate decreases as the velocity law becomes shallower with increasing β. Since emission processes often are proportional to ρ^2, an enhancement by a factor of $\eta_c \approx 3$ is sufficient to increase the emission by about an order of magnitude. For a velocity law with $\beta = 3$, this large increase in emission occurs if the rotation rate is about 11% critical. Below the $\eta_c = 2$ threshold, the winds are essentially spherical, so we define a WCZ as a stellar wind that has an equatorial compression with $\eta_c \geq 3$ formed by a star rotating slower than the WCD threshold.

Figure 4 shows specific examples of the effects of steep versus shallow velocity laws. Results for a WN5 wind with $\beta = 1$ (steep) and $\beta = 3$ (shallow) are shown in the leftward two columns. The compression of material toward the equator is illustrated in Figure 4 for three values of ω/ω_D. The streamlines originate from an evenly spaced grid in latitude with 10° intervals. The density of streamlines is an indication of the wind density. Near the star, the wind density decreases slower than r^{-2} for converging streamlines and faster than r^{-2} for diverging streamlines. Beyond a few stellar radii, the deflection of streamlines ceases, and the aspherical wind expands along radial trajectories. Figure 4*a* best represents the case for the O stars, which have high-speed winds and a fast acceleration to terminal speed. The wind in this case is little distorted from spherical. Figure 4*c* is the best representation of the Be stars, which have slower winds. Note that the flow lines terminate as they enter the equatorial plane; equator-crossing streamlines signal the formation of a dense disk in the WCD model of Be stars. Figure 4*e* represents a WCZ model for W-R winds. The wind acceleration law is slow, and even though a disk does not form, there is a significant compression near the equatorial plane at a rotation rate of only 16% critical. The results of these model calculations are summarized in Table 2.

Figure 5 shows the major increase in the density contrast as the rotation rate increases from 9% critical to 20% critical for a $\beta = 3$ velocity law (*left column*). Note from the second panel that even at a rotation rate of 16% critical,

TABLE 1

WCZ Model Parameters

Parameter	WN5[a]	B[e][b]	AGB[c]	Nova[d]
$T_{\rm eff}$(K)	66400	20100	2800	300000
$R_*/R_\odot$	3.7	86	510	0.01
$M_*/M_\odot$	10	37	5	1
log $L_*/L_\odot$	5.09	6.01	4.14	4.00
v_p	1775	810	30	560, 5560
$v_{\rm esc}$	930	270	60	5560
ζ	1.9	3.0	0.5	0.1, 1.0
$v_{\rm crit}$	660	190	40	3930
μ	1.30	0.86	1.30	0.94
μ_e	2.07	1.48	...	1.65
γ	0.5	0.35	0.35	0.35

[a] Stellar parameters are from Hamann et al. 1993; mean molecular weights are calculated using abundances from Nugis 1990 and ionization fractions from van der Hucht, Cassinelli, & Williams 1986.

[b] Stellar and wind parameters are from Cassinelli et al. 1989.

[c] Stellar parameters are from Livio 1994; abundances are discussed in the text.

[d] Typical white dwarf stellar parameters are assumed; abundances taken from Kato & Hachisu 1994.

TABLE 2

WCZ Results: The Wind Properties

Type	ζ	β	ω_D	ω	ω/ω_D	$\rho_{\rm eq}/\rho_p$[a]	$v_{\rm eq}/v_p$[a]	$\dot{M}_{\rm eq}/\dot{M}_p$[a]
WN5	1.9	1.0	0.64	0.32	0.5	1.9	0.82	1.6
				0.58	0.9	11.5	0.65	7.5
		3.0	0.18	0.09	0.5	2.3	0.95	2.2
				0.16	0.9	18.5	0.92	17.0
B[e]	3.0	1.0	0.90	0.45	0.5	1.7	0.81	1.4
				0.81	0.9	7.6	0.56	4.3
		3.0	0.36	0.18	0.5	2.3	0.93	2.1
				0.32	0.9	15.3	0.87	13.3
AGB	0.5	0.5	0.55	0.28	0.5	1.9	0.89	1.7
				0.50	0.9	9.3	0.78	7.3
		3.0	0.26	0.13	0.5	2.0	0.95	1.9
				0.23	0.9	14.7	0.91	13.5
Nova[b]	0.1	1.0	0.17	0.09	0.5	2.1	0.98	2.1
				0.16	0.9	12.8	0.97	12.4
		3.0	0.10	0.05	0.5	2.3	0.99	2.3
				0.09	0.9	10.5	0.98	10.3
	1.0	1.0	0.78	0.40	0.5	2.1	0.91	2.0
				0.71	0.9	14.3	0.83	11.7
		3.0	0.21	0.10	0.5	2.4	0.98	2.3
				0.19	0.9	18.7	0.96	18.0

[a] For each model the results are tabulated for wind properties at a radius of $10r_0$.

[b] Wind properties are computed for the case of $r_0 = 3R_*$.

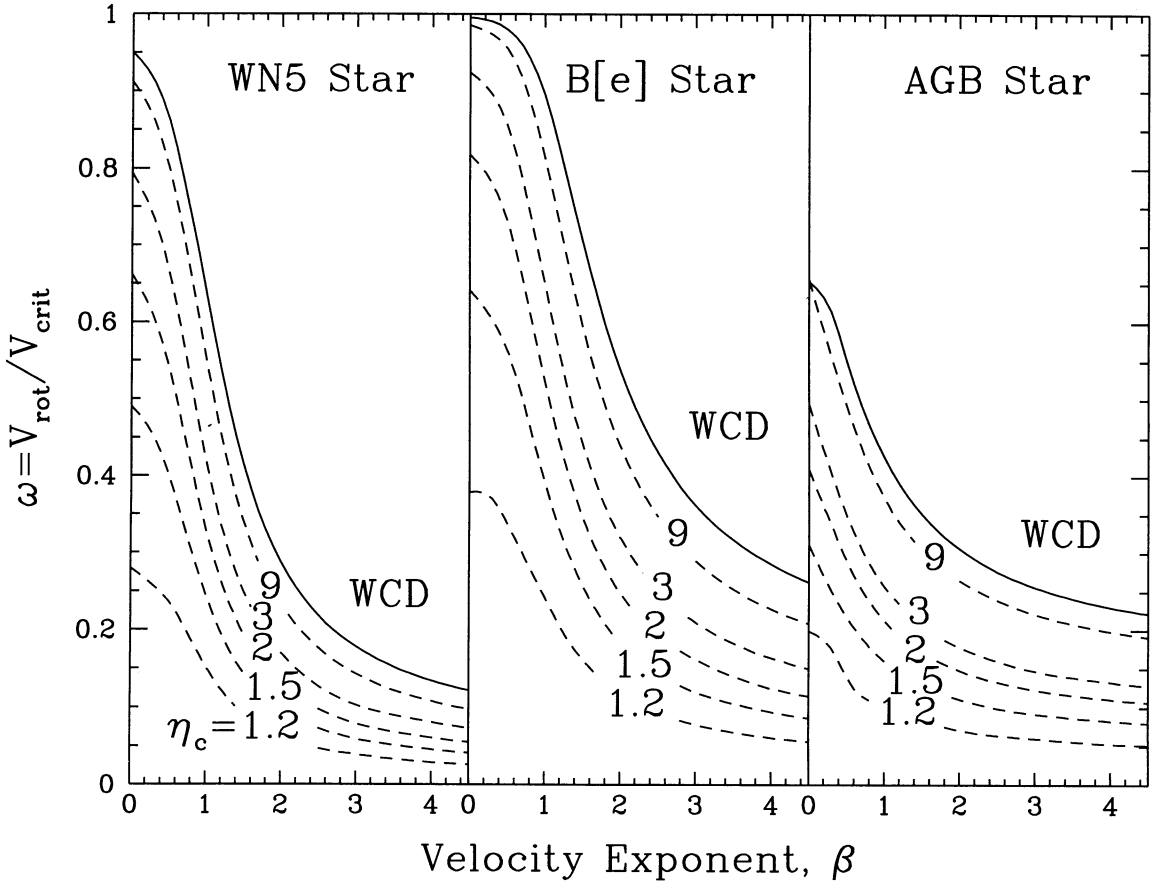

FIG. 3.—Rotation rate ω required for wind compression vs. the velocity law exponent β. The left panel is for a WN5 star, the middle panel is for a B[e] star, and the right panel is for an AGB star. The upper curve in each panel (*solid line*) corresponds to ω_D (the threshold value for forming a WCD). Along the lower curves (*dashed lines*), rotation will produce a density contrast between the equator and pole, $\eta_c = \rho_{eq}/\rho_p$, as indicated. These density contrasts are asymptotic values that occur at large radii. The intercept at $\beta = 0$ for each curve is controlled by the ζ-parameter and decreases as ζ becomes smaller. The ratio v_{esc}/v_s controls the right intercept, which decreases as v_{esc}/v_s becomes larger.

there will be a density contrast of almost 20. Note also that the density contrast increases rapidly in going from a rather slow rotation rate of 9% critical to a model that will have a disk at 20% critical. This result shows that very interesting equatorial enhancements can be attained at relatively low rotation rates.

Not all the W-R stars show intrinsic polarization, and this has been taken to indicate that rotation cannot be a major contributor to the W-R mass-loss process. However, even if that is the case, it is important to understand why some W-R stars show effects of rotation and others do not. Our models provide a plausible explanation for this. If we use the threshold values from our models, and if we assume that the rotation rates of W-R stars follow a distribution function such that some fraction have rotation rates larger than our WCZ threshold of about 11% critical, then the more rapidly rotating W-R stars will have a WCZ wind structure, while those that rotate more slowly will not.

In addition to the occurrence of polarization among the W-R stars, this hypothesized distribution function may have relevance for another observational conundrum among the W-R stars. It is known that only some WC8 stars show evidence for dust in their winds, whereas nearly all the cooler WC9 stars have dust (Williams 1995). In the context of the idea that there exists a distribution of WR rotation speeds, perhaps dust formation in the WC8 winds can begin at the equator for some minimum equatorial density enhancement corresponding to a particular rotation threshold. The cooler WC9 stars, on the other hand, do not require any density enhancement for dust condensation to occur.

4.2. B[e] *Stars*

The B[e] stars are another class of hot stars that exhibit aspherical mass loss, as inferred from spectroscopic observations (Zickgraf et al. 1985, 1986). They differ from the classical Be stars treated in BC in that Be stars are of luminosity classes V to III, while the B[e] stars are supergiants. The B[e] stars show strong (often P Cygni) Balmer emission lines as well as low ionization state permitted and forbidden emission lines (e.g., [O I] and [Fe II]). The B[e] stars also exhibit IR excesses from the reprocessing of stellar radiation by circumstellar dust (Allen & Glass 1976).

Zickgraf et al. (1985, 1986) have advocated a wind model with an equatorially enhanced density to explain the various features observed in the spectra of B[e] stars. They suggest that the equatorial wind enhancement is produced by an expulsion of material owing to rapid stellar rotation. Although the occurrence of rapid rotation among evolved supergiants may seem unlikely, the B[e] stars are located close to the Humphreys-Davidson limit in the H-R diagram, so the surface gravity at the star should be greatly diminished by the radiation pressure, and the critical rotation speed will also be significantly reduced (Cassinelli et al.

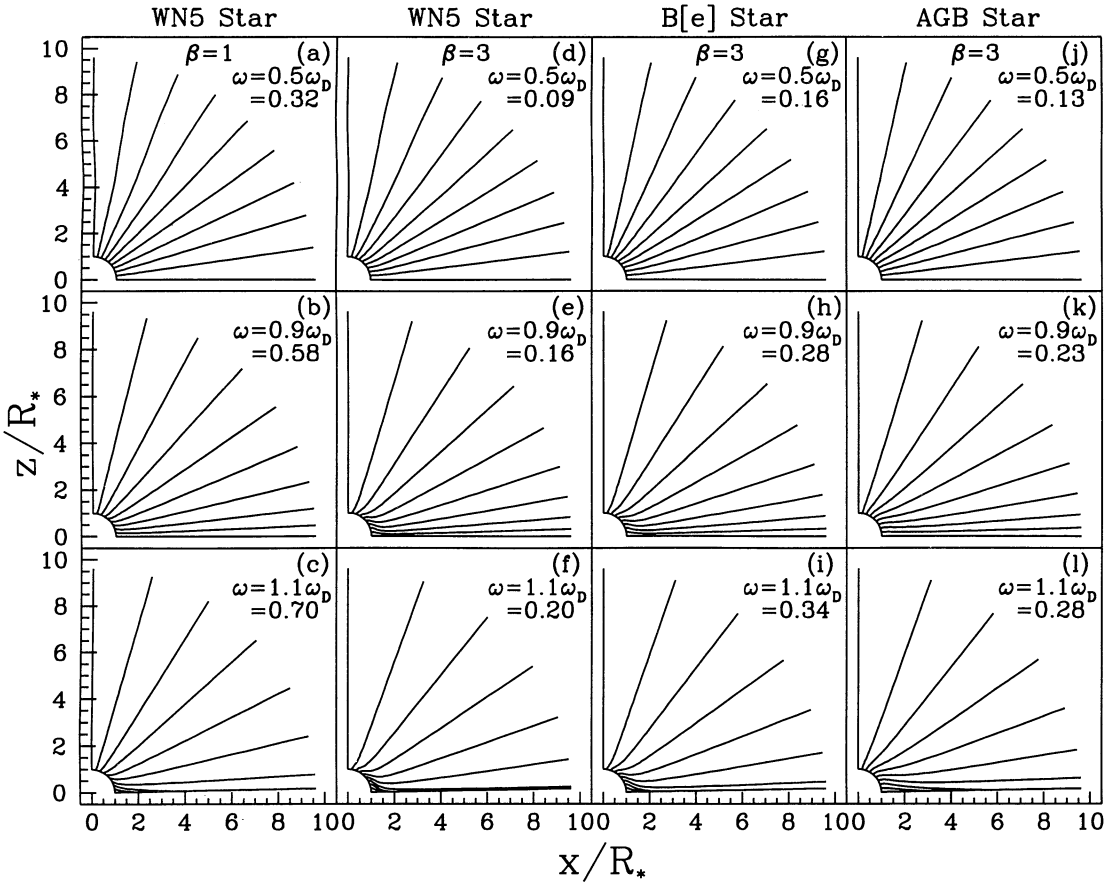

FIG. 4.—Streamlines for various values of the rotation rate $\omega = v_{rot}/v_{crit}$ in a WN5 stellar wind, a B[e] wind, and an AGB wind. The coordinates z and x are cylindrical coordinates, where z is the height above the equatorial plane and x is the polar radial coordinate measured perpendicular to the z-axis. The streamlines originate at 10° increments in latitude, and the separation between the streamlines is an indication of the density in the wind. The leftmost column shows results for a steep velocity law ($\beta = 1$) in a WN5 stellar wind. From left to right, the remaining three columns are results for a shallow velocity law ($\beta = 3$) in a WN5 wind, a B[e] wind, and an AGB wind, respectively. On each plot we list the rotation rate, both as a fraction of the disk formation threshold, ω_D, and as a fraction of the critical rotation speed. From top to bottom, the wind structure becomes progressively more equatorially compressed as the stellar rotation speed is increased. Moving from left to right, notice how the wind structure remains relatively constant independent of stellar type and β-value as long as ω/ω_D is held constant. Note also that significant wind distortions are achieved at much lower stellar rotation rates for $\beta = 3$ than for $\beta = 1$.

1989). For the B[e] stars, the breakup speed of rotation is only about 200 km s^{-1}. Several rotational models have already been developed for B[e] stars (Lamers & Pauldrach 1991; Cassinelli et al. 1989). These models require rotation rates rather near the critical speed. As was the case for the W-R stars, we find that by accounting for wind compression, large density enhancements can occur at much smaller rotation rates.

We have calculated wind compression models for B[e] stars using the stellar and wind parameters listed in Table 1. A plot of the WCD threshold rotation rates and the rates needed for a range of density enhancements is shown in the middle panel of Figure 3. Comparing the results for the B[e] star to that shown for the WN5 star, we find that the WCD and WCZ threshold curves are similar in shape as a function of β; however, the thresholds are significantly larger at all β for the B[e] star than for the WN5 star. This is because ζ is larger and v_{esc}/v_s is smaller in the B[e] winds, and these two parameters set the scale of the rotation thresholds (eqs. [13] and [15]).

Results of our model simulations for $\beta = 1$ and $\beta = 3$ are given in Table 2. For $\beta = 1$, a rapid rotation in excess of 90% critical is required for disk formation, but a rotation of 60% critical will result in a WCZ. These rotation rates correspond to speeds of about 170 and 110 km s^{-1}, respectively. Note that if the star rotates as rapid as 90% critical, the bi-stability mechanism (Lamers & Pauldrach 1991) or magnetic forces (Cassinelli et al. 1989) can further enhance the stellar mass loss in the equatorial region.

Although $\beta \approx 1$ is normally assumed, Massa et al. (1995) find that a shallower wind velocity law may be realized in some B supergiant winds, so WCZ results for large β-values may be relevant to evolved B stars. Examples of the wind flow structure and density distribution for the B[e] star in the case of $\beta = 3$ are shown in panels Figures 4*g*–4*i* and 5*d*–5*f*. Note the similarity of the asymptotic wind properties at a fixed value of the ratio ω/ω_D. With $\beta = 3$, the rotation threshold for a WCD and WCZ are around 40% and 20% critical, which are reduced relative to the $\beta = 1$ thresholds by more than a factor of 2. In this case, the stellar rotation is small enough that other mechanisms for producing additional mass loss from the equator are probably not effective.

The widths of the emission lines from the B[e] winds provide an important constraint to the wind models. The observations suggest that the pole to equator terminal speed ratio, v_p/v_{eq}, is of order 10. From Table 2, none of the WCZ wind models for B[e] stars are able to reproduce a ratio v_p/v_{eq} of this magnitude. However, a v_p/v_{eq} ratio of the correct order is attainable in a WCD (see Owocki et al. 1994) or in a bi-stable wind (see Lamers & Pauldrach 1991).

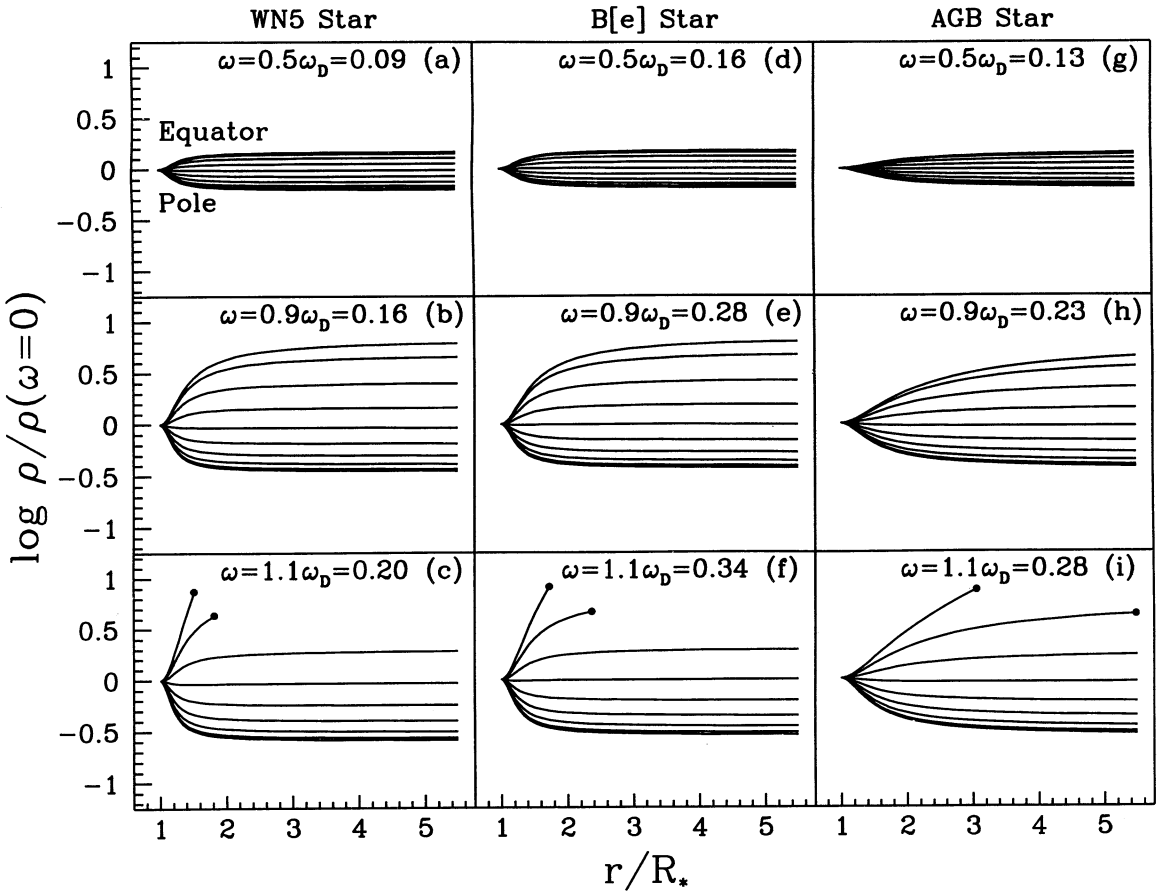

FIG. 5.—Ratio of the density in wind-compressed models to that of nonrotating models as a function of distance from the star for the streamlines shown in Fig. 4. For each star the wind density is computed at three different stellar rotation speeds, each of which is listed in terms of the disk-forming rotation, ω_D, and in terms of the critical rotation speed. A shallow velocity law with $\beta = 3$ is used for all these models. In the lower panel, dots mark the termination of streamlines entering the disk, where the density may increase by ~ 2 orders of magnitude (not shown).

If the B[e] phenomenon is to be explained by rotational effects, these stars must rotate fairly rapidly (greater than 40%–50% critical for most reasonable β-values) to reproduce $v_p/v_{eq} \approx 10$. On the other hand, if γ is greater than 0.35 for B[e] stars, the wind terminal speed at the equator will be more sensitive to ω. To obtain $v_p/v_{eq} \approx 10$ at a rotation below the disk threshold, we find that γ must increase by nearly 2 orders of magnitude, which is unrealistically high, suggesting that rapid stellar rotation is likely required to explain the spectral observations of B[e] winds.

4.3. *Asymptotic Giant Branch Stars*

Stars destined to become white dwarfs will first pass through an AGB phase and then a PN phase. Observations show that PNe form a rich morphological sequence, ranging from spherical, to elliptical, to strongly bipolar (Balick 1987). To explain the aspherical nebular morphologies, Kahn & West (1985) and Icke (1988) developed simplified analytical models that describe a wind bubble formed by a fast, spherical wind from the central star of a PN that has been injected into a slow, dense axisymmetric wind from a precursor phase. More recently, Frank & Mellema (1994) considered numerical gasdynamical simulations of interacting winds in PNe. Allowing for a variety of density contrasts and viewing angles, they were able to reproduce most of the observed morphologies and radial velocity maps from their models. They conjecture that the nonspherical distribution of material from the PN progenitor must result from the superwind during the AGB phase. Thus, there appears to be a need for forming equatorially enhanced winds from AGB stars, and here we investigate conditions under which the WCZ models could provide sufficient equatorial compression.

The AGB winds are the first example of a stellar wind in our study that is not principally line driven. Instead, the AGB stars have dust-driven winds. The winds are massive because stellar pulsations create an extended atmosphere that greatly increases the gas density near the dust condensation radius (Bowen 1988). To the extent that the WCZ model assumptions are satisfied (i.e., central forces, radial flow through the subsonic region, and a β-velocity law for the supersonic flow; see § 2.1), the AGB stars are candidates for having a rotationally induced wind distortion. A series of WCZ models has been calculated using AGB stellar and wind parameters listed in Table 1. An AGB star with a main-sequence mass of 5 $M_\odot$ is chosen, and it is assumed that the star has retained all its main-sequence mass up to the AGB phase. For the mean molecular weight, μ, we assume a wind that is composed of 90% H, 9% He, and 1% metals (by number), and we assume that hydrogen and helium are neutral. Since the electron scattering opacity is expected to be negligible in the AGB winds, an entry for the mean molecular weight per free electron, μ_e, is not given in the table.

The rightmost panel of Figure 3 shows the disk formation threshold, ω_D, as a function of β. In comparison with the WN5 star, ω_D is smaller for the AGB wind by a factor of 0.7 at low β, but it is larger by a factor of nearly 2 at high β. The former is a consequence of smaller ζ-values for AGB winds than for WN5 winds. At high β, the ratio v_{esc}/v_s is smaller in the AGB winds than the WN5 winds, so ω_D is higher, and the AGB star must rotate at a greater fraction of v_{crit} to form a disk than does a WN5 star. In comparison to the B[e] star, ω_D is smaller for the AGB wind at low β, but for large β, both stars have nearly equal disk thresholds owing to the fact that v_{esc}/v_s is comparable between the two stars.

The density and flow structure of a rotating AGB star have been computed for $\beta = 0.5$ and $\beta = 3$, and the results are given in Table 2. From this table, a wind density contrast of about 2 (sufficient to account for many PN shapes) is achieved with a stellar rotation of 28% critical for $\beta = 0.5$, but only 13% critical at $\beta = 3$. Disk formation occurs at 55% critical for $\beta = 0.5$ and only 26% critical for $\beta = 3$.

The wind flow structure for the $\beta = 3$ case is shown in Figures 4*j*–4*l* at three different stellar rotations. Once again, we point out the large degree of symmetry exhibited in the asymptotic wind structure between the different stars. Figure 5 shows the corresponding density structure for the AGB wind models of Figure 4. As compared with the WN5 and B[e] stars, the distorted density structure of the AGB star appears to be more "extended." Whereas the other stellar winds obtain their asymptotic structure within a stellar radius, the distortion of the AGB wind takes place over a span of three to four stellar radii. This is due to the radically different length and speed scales between the three stars. Even with these differences, we note that the asymptotic wind structure (i.e., density contrast and streamline positions) is comparable at fixed values of ω/ω_D for these stars with very dissimilar wind properties.

The wind structures relevant for the AGB winds are those that achieve a density contrast of 2 or more. Our models require a stellar rotation rate that is only of order 10% critical ($\beta = 3$) to obtain $\eta_c = 2$. With this rotation rate, the wind-wind interaction between the central star of the PN and the AGB star will likely produce an axisymmetric bubble that is significantly ellipsoidal, with the greatest extension along the axis of rotation. For more rapidly rotating AGB stars, the equatorial compression will be stronger, so the PN bubble will have a greater extension along the symmetry axis (i.e., the bubble will have a greater degree of bipolarity). However, even the low stellar rotation rate of 10% critical is higher than one would expect for a single AGB star, with likely values of ω ranging from 0.01%–0.1% critical (Livio 1994).

This problem of insufficient angular momentum may be solved if the AGB star has a binary companion. Livio & Soker (1988) have shown that the outer layers of the AGB stellar atmosphere can be "spun-up" during a common envelope phase. In some cases a massive Jupiter-like planet ($M \sim 10 M_{Jup}$) may be sufficient to spin-up an AGB star in excess of 35% critical (Soker 1994; Livio 1994). The idea that a massive planet could increase the rotation rate of an AGB star is attractive, since the formation of planets may be a common occurrence among stars (Beckwith et al. 1990; O'Dell, Wen, & Hu 1993).

To summarize, it is unlikely that stellar rotation could induce an aspherical distortion in the winds of single AGB stars. However, in a binary system, an AGB star could be spun-up by a companion object. The degree of ellipticity or bipolarity in the PN is subject to how much the AGB star is spun-up, which in turn depends on the details of the binary system, such as the dimensions and separation of the two objects and their masses (Livio 1994). The combination of a spin-up by a low-mass binary companion and wind-compressional effects may explain the source of AGB wind asphericities inferred by the observations of PN morphologies.

At this point, we interject a cautionary note regarding our results for the AGB stars. The effects of dust are important in driving the AGB winds, and two-fluid hydrodynamic models for both the dust and gas of AGB winds indicate that (1) the sonic point may occur beyond the stellar surface, and (2) the supersonic flow may not be described by a shallow wind acceleration (Netzer & Elitzur 1993; Habing, Tignon, & Tielens 1994). To truly investigate wind compression effects in these stars requires a model of the transonic wind flow. We note, however, that for C-rich AGB stars, the base of the wind is sometimes observed to occur near the stellar surface (Lucy 1976).

4.4. *Novae*

Classical novae occur in close binary systems consisting of a white dwarf and a nondegenerate companion (Gallagher & Starrfield 1978). Mass transfer from the companion star to the white dwarf leads to an accretion disk and the production of a hydrogen-rich envelope on the white dwarf. A thermonuclear runaway in the hydrogen-rich envelope rapidly ejects a shell of gas (Starrfield, Truran, & Sparks 1978) that can obtain speeds up to a few thousand km s^{-1} with a total mass of 10^{-5} to 10^{-4} $M_\odot$. However, not all the accreted material will be ejected in the outburst. Some material will remain and develop an extended envelope with a radiation pressure–driven wind (Bath & Shaviv 1978; Ruggles & Bath 1979; Kato 1983). Although most theoretical models of nova outbursts assume spherical symmetry, many novae are observed to be aspherical, such as GK Per (Duerbeck & Seitter 1987) and Nova Cyg 1992 (Bjorkman et al. 1994; Paresce 1994). The possibility that magnetic fields could play a role in the nova phenomenon was considered by Collins & Foltz (1977) and Orio, Trussoni, & Ögelman (1992). Collins & Foltz suggest a mechanism whereby magnetic effects will induce a polar ejection for almost any nova-like system, but the mechanism requires that the white dwarf mass be close to the Chandrasekhar limit. The results of Orio et al. are most applicable to AM Herculis types and intermediate polars which typically have strong surface magnetic fields. Nova white dwarfs that do not have large magnetic fields and whose masses are not close to the Chandrasekhar limit may still rotate at moderate rates, perhaps in excess of 20% critical (Sion et al. 1995). So, we investigate whether the observed asymmetries in novae may be induced by rotational wind compression effects alone.

The nova outburst is significantly different from other stars that we have considered in that the nova wind can have an extended subsonic zone whose properties evolve with time. In considering wind compression effects for novae, we make the following assumptions. First, we compute wind models for a sequence of release point radii, because the sonic radius moves as the nova evolves. Since we are mainly interested in limits on the rotation rate of the

white dwarf, we require an angular momentum distribution for the subsonic zone, which we assume to be angular momentum conserving. In this case, $v_{\rm rot} \propto r^{-1}$, and because $v_{\rm crit} \propto r^{-1/2}$, the rotation rate at the sonic point can be related to the white dwarf rotation rate by $\omega_D(R_*) = (r_s/R_*)^{1/2}\omega_D(r_s)$.

Second, we assume that $\zeta = v_\infty/v_{\rm esc}$ is a constant, where $v_{\rm esc}$ is the local escape speed at the sonic point. Consequently, although ζ is held constant in our wind models, the terminal speed decreases with increasing sonic point radius. Since we do not know the value of ζ as a function of the sonic point radius, we compute two sets of models: the first with a small value of $\zeta = 0.1$ and the second with a larger value of $\zeta = 1.0$.

Finally, Kato & Hachisu (1994) have published new theoretical models for spherical optically thick winds from novae. In their picture, the wind is accelerated by a locally super-Eddington luminosity that occurs in a region in which the opacity experiences a large increase because of iron lines (see Iglesias & Rogers 1991). Since the iron line opacity occurs at a temperature of 3×10^5 K, we use this temperature for computing the sound speed in all our models.

Adopting stellar parameters for a typical white dwarf star and a luminosity for a typical nova (see Table 1), we have computed wind compression models for a range of sonic point radii from $r_s = R_*$ up to $20R_*$. Note that the $T_{\rm eff}$ listed in Table 1 is the temperature *at the sonic point*, and the terminal speed of the wind is given for the two values of ζ, 0.1 and 1.0. Figure 6 shows the threshold rotation rate at the white dwarf surface, $\omega(R_*)$, for a WCD and a WCZ plotted as a function of the sonic point radius, r_s. The upper panel corresponds to $\zeta = 0.1$, while the lower is for $\zeta = 1.0$.

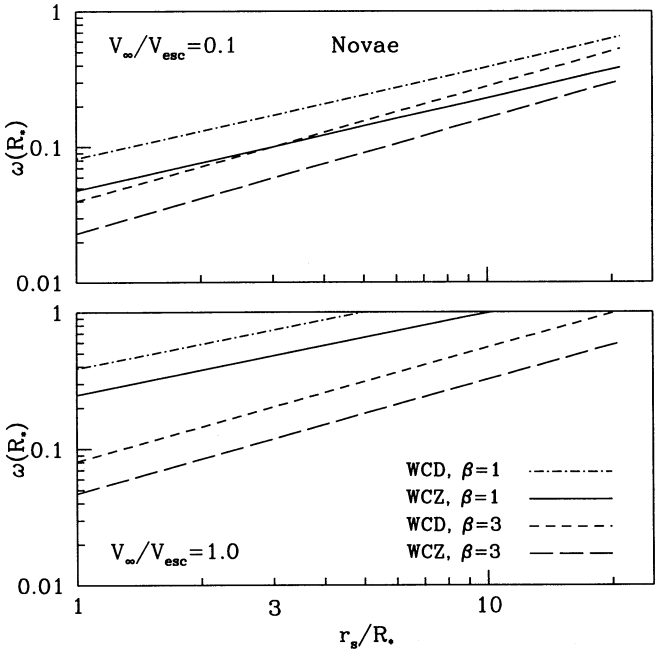

FIG. 6.—The rotation rate of the nova white dwarf plotted as a function of the sonic point radius, r_s. *Top:* $\zeta = v_\infty/v_{\rm esc} = 0.1$; *bottom:* $\zeta = 1.0$. As indicated, the different line types are for the WCD and WCZ threshold rotation rates with $\beta = 1$ or 3. For $r_s/R_* \gg 1$, the white dwarf must rotate at near-critical speeds for wind compression effects to be significant, and this is independent of the value of either ζ or β. The lowest thresholds occur when the sonic point is close to the stellar surface, the terminal speed is low, and β is large.

In each of these panels, two cases are shown: one for $\beta = 1$ and the other for $\beta = 3$. Figure 6 indicates that as the sonic point moves outward to large radii, the white dwarf must rotate faster (approaching near-critical speeds) to form a significant equatorial compression, independent of either ζ or β. Significant wind distortions are thus more likely to occur for sonic point radii that are closer to the white dwarf. Moreover, the threshold rotation rates are minimized for small terminal speeds and large velocity exponents.

Results of the wind compression models are listed in Table 2 for $r_s = 3R_*$. We find that for $\zeta = 0.1$, disk formation occurs at 17% and 10% critical for $\beta = 1$ and 3, respectively. If $\zeta = 1$, the white dwarf must rotate at 78% critical to form a WCD for the case of $\beta = 1$ but only 21% critical if $\beta = 3$. So, interesting equatorial compressions are achievable at rotation rates of 10%–20% critical for small sonic point radii. Since low wind terminal speeds decrease the threshold rotation rate, our wind compression models may have greatest applicability for "slow" novae, which lose mass primarily via sustained winds that have small terminal speeds with $v_\infty \lesssim 500$ km s^{-1}. DQ Her and HR Del are examples of slow novae that both have highly asymmetric shells (Mustel & Boyarchyk 1970; Solf 1983).

Further investigations of the rotational effects in nova winds must account for two effects that we have ignored. First, if a significant equatorial compression does form in the optically thick nova envelope, a latitudinal torque will develop owing to asymmetries in the radiation pressure force. Such a torque will tend to resist the wind compression itself. A poleward radiative torque is known to reduce the equatorial compression in the case of stellar oblateness (Cranmer & Owocki 1995), consistent with our expectations for the optically thick case.

Second, the extended transonic flow should be properly modeled. Figure 6 shows the large sensitivity of our quantitative results for the rotation thresholds to the location of the sonic point (or equivalently, the release point r_0). Since, for large values of β, the transonic zone is extended for WR, B[e], and AGB stars, this figure also illustrates the sensitivity of our rotation thresholds to the location of the release point for these stars as well.

Finally, it is interesting to note that the optically thick wind models of Kato & Hachisu (1994) exhibit extremely shallow velocity laws in an extended subsonic zone. With our supersonic wind model, we have demonstrated that shallow velocity laws tend to increase the sensitivity of the wind to rotational distortion. If this trend should also hold for the subsonic flow, equatorial compressions might begin to form in the subsonic zone prior to the point of release into the supersonic flow.

5. SUMMARY

The purpose of this paper has been to assess whether rotational wind effects might be important for widely differing stellar conditions across the H-R diagram. We have used the kinematic, two-dimensional WCD model to investigate how the wind distortion is affected by the wind acceleration. The model results are applied to a Wolf-Rayet star, a B[e] star, an AGB star, and a nova white dwarf. Some stars in each of these classes exhibit aspherical mass loss, but the observations do not necessarily indicate the presence of an extremely dense circumstellar disk. Consequently, we have also chosen to study wind models that result in significant ($\gtrsim 3$) equatorial to polar density contrasts (WCZ

models) without the formation of a WCD. Three main conclusions have been reached.

1. The rotation threshold for disk formation is set by three fundamental parameters: v_{rot}, v_∞, and β. If the wind acceleration is large, significant wind distortions can result only if the star is rapidly rotating. However, wind distortions will also occur for slow to moderate stellar rotation rates if the wind acceleration is small. In the context of a β-velocity law, small wind accelerations result in two ways: (1) The wind acceleration scales as v_∞, so if v_∞ is small, the wind acceleration is small or (2) even if v_∞ is large, a high value of β will result in a small wind acceleration near the star (i.e., a shallow velocity law). In both cases, the outward flow speed of the wind in the vicinity of the stellar surface is small compared to the critical speed of rotation, so there can be a significant deflection of the wind toward the equator, leading to an equatorial density enhancement. Note that for $\beta \gg 1$, the sound speed, v_s, becomes crucial in determining the equatorial compression because the velocity law becomes quite shallow near the sonic point. Greater density contrasts are achieved for smaller values of v_s.

2. The WCZ model was applied to several different cases, the results of which are recapitulated here.

WN5 stars.—If the wind velocity is described by a $\beta = 3$ law, we find that a substantial equatorial wind compression ($\eta_c \sim 20$) can form at a rotation rate of only 16% critical. Not only do significant density contrasts result for relatively small rotation rates, but the wind compression is also sensitive to small changes in ω. This sensitivity to the rotation rate may explain why only a fraction of W-R stars are intrinsically polarized. We suggest that there is a distribution function representing the number of W-R stars with a given ω, for which most W-R stars are slow rotators with effectively spherical winds. A few W-R stars, however, rotate fast enough to induce an aspherical wind that can be observed polarimetrically and can influence the formation of dust grains among the WC8 stars.

B[e] *stars.*—The spectrum of a B[e] star displays broad Balmer emission lines and narrower low ionization emission lines. If these observations are to be explained by a wind geometry containing a fast polar wind and a slow, dense equatorial disk, the pole to equator terminal speed ratio, v_p/v_{eq}, must be of order 10. To produce such a large terminal speed ratio with our wind compression model will likely require a WCD. If the B[e] winds are represented by a $\beta = 1$ velocity law, a rotation rate of 90% critical (i.e., $v_{rot} \approx 170$ km s^{-1}) is needed to form a WCD. For this near-critical rotation rate, other effects will contribute to the equatorial density enhancement, such as the bi-stability mechanism or magnetic effects (Lamers & Pauldrach 1991; Cassinelli et al. 1989). On the other hand, if $\beta = 3$, the disk formation threshold drops to 36% critical, for which v_{rot} is only 70 km s^{-1}.

AGB stars.—In the interacting winds scenario for PN formation, a density contrast of 2 or 3 is sufficient to reproduce the wide variety of elliptical and bipolar morphologies. We find that density contrasts of 2–3 can result from rotations of order 15% critical if the wind acceleration is described by a $\beta = 3$ law. Even if the AGB winds have steep velocity laws, these density contrasts can be obtained with stellar rotations of order 30% critical. Although a rotation of 15% critical is too rapid to occur in single AGB stars, Livio (1994) has demonstrated that an AGB star may be "spun-up" to $\omega \gtrsim 35\%$ critical by a low-mass companion (perhaps as small as a massive planet) during a common envelope phase. At a rotation rate of 35% critical, wind-compressional effects should be significant. Since our current model does not properly account for the extended subsonic regions that may exist in AGB winds, our conclusions about rotation rates are only qualitative. More detailed calculations are required to incorporate the subsonic structure.

Novae.—Following a nova outburst, a white dwarf star can retain an extended envelope with a radiation driven wind. However, the nova winds are significantly different from the other objects considered in this investigation in that the wind properties (terminal speed, sonic point radius, mass-loss rate) evolve with time. To determine whether wind compression effects have relevance for novae, we have computed WCZ models for a range of sonic point radii. We find that significant equatorial compressions may result for stellar rotation rates $\omega < 20\%$ critical if (1) the sonic point is close to the white dwarf surface, (2) the wind terminal speed is small, or (3) the velocity exponent, β, is large. In particular, the wind compression model may have relevance for slow novae, which tend to maintain winds with low terminal speeds (a few hundred km s^{-1}) throughout their outburst.

3. An unexpected result of our calculations is that for a fixed value of ω/ω_D, WCZ models with different stellar parameters and different velocity exponents show strikingly similar asymptotic wind properties (flow pattern and density contrast). This similarity property could be useful in simplifying and generalizing the application of the WCZ model to a wide variety of stars. An implication of this property is that one could compute a series of rotating wind models for a sequence in ω/ω_D, and the results would be applicable to any star (to zero order). In a subsequent paper, we will present approximations to the WCZ model that allow for a rapid and accurate computation of the rotating wind structure, and this similarity property will be discussed in more detail.

In conclusion, rotationally induced wind distortions, either alone or in conjunction with other mass-loss mechanisms, appear to have broad application to stars throughout the H-R diagram. Wind compression effects can be significant, even if a disk does not form.

However, one problem with our current model is that it does not account for either an extended subsonic or transonic region of the flow. The hydrodynamical models of Owocki et al. (1994) have demonstrated that the subsonic region is effectively corotating and that the deflection of streamlines should be computed *from the sonic point*, but in their models the subsonic and transonic zones were narrow. If the subsonic or transonic zones are extended with scale heights of order a stellar radius, the WCD and WCZ threshold rotation rates presented here will likely have to be altered, but to what extent will depend on the angular momentum transport and the deflection of streamlines as gas pressure support is lost through these region (see our nova case, which illustrates the sensitivity to the location of the release point). The threshold rotation rates predicted by the current model are probably accurate for small β-values but less accurate for the high-β cases. A solution to the subsonic and transonic wind structure would complete our wind model and allow for better estimates of the threshold rotation rates at which wind-compressional effects become important.

We would like to thank Adam Frank and Joni Johnson for helpful discussions about planetary nebulae and AGB stars. We also thank Jay Gallagher, Marina Orio, and Sumner Starrfield for their information about novae. Finally, we thank Stan Owocki for many helpful comments and suggestions. This research was supported by the NASA grants NAG5-2854 and NAGW 2210 and the NSF grant AST-9115375.

APPENDIX A

DERIVATION OF THE STREAMLINE TRAJECTORIES

Here we derive the equation describing streamline trajectories in the orbital plane. The differential equation governing the fluid motion in the orbital plane is found from taking the ratio of v'_ϕ to v'_r (eqs. [4] and [2]). Letting $r' = r$ and setting $v_\infty = v_\infty(\theta_0)$, the equation of motion is

$$\frac{d\phi'}{dr} = \frac{r_0}{r^2} \frac{v_{\rm rot} \sin \theta_0}{v_0 + (v_\infty - v_0)(1 - r_0/r)^\beta}, \tag{A1}$$

where ϕ' is the azimuthal coordinate in the orbital plane and is referred to as the "deflection."

To integrate expression (A1), we make a change of variable from the spatial coordinate, r, to the velocity, v_r. Recall that $v_r = v_0 + (v_\infty - v_0)(1 - r_0/r)^\beta$, so

$$dv_r = \beta \frac{r_0}{r^2} (v_r - v_0)^{1/\beta} (v_\infty - v_0)^{1 - 1/\beta} dr . \tag{A2}$$

Rewriting equation (A1) in terms of v_r and integrating over dv_r, we find that

$$\phi' = \frac{v_{\rm rot} \sin \theta_0}{\beta} (v_\infty - v_0)^{-1/\beta} \int_{v_0}^{v_r} v_r^{-1} (v_r - v_0)^{1/\beta - 1} dv_r , \tag{A3}$$

where $\phi'(r = r_0)$ has been set to zero.

Denoting the integral appearing in equation (A3) as I, the integrand can be rearranged such that

$$I = \int_{v_0}^{v_r} v_r^{1/\beta - 2} (1 - v_0/v_r)^{1/\beta - 1} dv_r . \tag{A4}$$

Making a change of variable, $t = 1 - v_0/v_r$, this integral becomes

$$I = \int_0^{1 - v_0/v_r} v_0^{1/\beta - 1} t^{1/\beta - 1} (1 - t)^{-1/\beta} dt , \tag{A5}$$

which is the incomplete beta function, $B_y(1/\beta, 1 - 1/\beta)$, multiplied by the constant, $v_0^{1/\beta - 1}$, where the upper limit $y = 1 - v_0/v_r$. Combining equations (A3) and (A5) and setting $v_0 = v_s$ (the sound speed) and $r_0 = R_*$ (the stellar radius), the azimuthal deflection is seen to be

$$\phi' = \frac{v_{\rm rot} \sin \theta_0}{\beta v_s} \left(\frac{v_s}{v_\infty - v_s} \right)^{1/\beta} B_y \left(\frac{1}{\beta}, 1 - \frac{1}{\beta} \right) . \tag{A6}$$

APPENDIX B

DERIVATION OF THE WIND DENSITY DISTRIBUTION

From the consideration of a streamtube and the equation of mass continuity, the expression for the wind density is (see eq. [8])

$$\rho = \frac{\dot{M}_0}{4\pi r^2 v_r(r, \theta_0)} \left(\frac{d\mu}{d\mu_0} \right)^{-1} , \tag{B1}$$

where $\mu = \cos \theta$ and $\mu_0 = \cos \theta_0$. Following BC, the wind compression factor, $d\mu/d\mu_0$, is derived from the coordinate transformation between the orbital coordinates and the stellar coordinates:

$$\mu = \mu_0 \cos \phi' . \tag{B2}$$

Differentiating equation (B2) yields

$$\frac{d\mu}{d\mu_0} = \cos \phi' + \phi' \sin \phi' \left(\frac{1 - x_0^2}{x_0^2} \right) \frac{d \ln \phi'}{d \ln x_0} , \tag{B3}$$

where $x_0 = \sin \theta_0 = (1 - \mu_0^2)^{1/2}$. The derivative appearing in the second term of equation (B3) can be evaluated by differenti-

ating ϕ' in equation (A6), giving

$$\frac{d\ln\phi'}{d\ln x_0} = 1 - \frac{d\ln v_\infty}{d\ln x_0}\left(\frac{v_\infty}{v_\infty - v_s}\right)\left[\frac{1}{\beta} - \frac{1}{B_y}\frac{(v_r/v_s - 1)^{1/\beta}}{v_r/v_s}\right]. \tag{B4}$$

From equation (25) of BC, the factor $d\ln v_\infty/d\ln x_0$ is

$$\frac{d\ln v_\infty}{d\ln x_0} = \frac{-\gamma\omega x_0}{1-\omega x_0}. \tag{B5}$$

Back-substitution of equations (B3)–(B5) into equation (B1) will yield the full expression for the wind density as a function of r, θ_0, and $v_r(r, \theta_0)$.

REFERENCES

Abramowicz, M., & Stegun, I. A. 1972, Handbook of Mathematical Function (New York: Dover)
Allen, D. A., & Glass, I. S. 1976, ApJ, 210, 666
Auer, L. H., & Koenigsberger, G. 1994, ApJ, 436, 859
Balick, P. L. 1987, AJ, 94, 671
Barlow, M. J., Smith, L. J., & Willis, A. J. 1981, MNRAS, 196, 101
Bath, G. T., & Shaviv, G. 1978, MNRAS, 175, 303
Beckwith, S. V. W., Sargent, A. I., Chini, R. S., & Güsten, R. 1990, AJ, 99, 924
Bjorkman, J. E., & Cassinelli, J. P. 1993, ApJ, 409, 429 (BC)
Bjorkman, K. S. 1989, Ph.D. thesis, Univ. Colorado
Bjorkman, K. S., Johansen, K. A., Nordsieck, K. H., Gallagher, J. S., & Barger, A. J. 1994, ApJ, 425, 247
Blondin, J. M., & Lundqvist, P. 1993, ApJ, 405, 337
Bowen, G. H. 1988, ApJ, 329, 299
Cassinelli, J. P. 1991, in IAU Symp. 143, Wolf-Rayet Stars and Interrelations with other Massive Stars in Galaxies, ed. K. A. van der Hucht & B. Hidayet (Dordrecht: Kluwer), 289
Cassinelli, J. P., Schulte-Ladbeck, R. E., Poe, C. H., & Abbott, M. 1989, in Physics of Luminous Blue Variables, ed. K. Davidson, A. F. J. Moffat, & H. J. G. L. M. Lamers (Dordrecht: Kluwer), 121
Chevalier, R. A., & Luo, D. 1994, ApJ, 421, 225
Collins, G. W., & Foltz, C. B. 1977, PASP, 89, 896
Coté, J., & Waters, L. B. F. M. 1987, A&A, 176, 93
Coyne, G. V., & McLean, I. S. 1982, in IAU Symp. 98, Be Stars, ed. M. Jaschek & H.-G. Groth (Dordrecht: Reidel), 77
Cranmer, S. R., & Owocki, S. P. 1995, ApJ, 440, 308
dos Santos, L. C., Jatenco-Pereira, V., & Opher, R. 1993, ApJ, 410, 732
Duerbeck, H. W. 1987, Space Sci. Rev., 45, 1
Duerbeck, H. W., & Seitter, W. C. 1987, Ap&SS, 131, 467
Dupree, A. K. 1986, ARA&A, 24, 377
Ebbets, D., White, R., Walborn, N., Davidson, K., & Malumuth, E. 1992, in ESO Conf. 44, Science with the Hubble Space Telescope, ed. P. Benvenuti & E. Schreier (München: ESO), 395
Frank, A., & Mellema, G. 1994, ApJ, 430, 800
Friend, D. B., & Abbott, D. C. 1986, ApJ, 311, 701
Friend, D. B., & Castor, J. I. 1982, ApJ, 261, 293
Gallagher, J. S., & Starrfield, S. 1978, ARA&A, 16, 171
Gayley, K. G., Owocki, S. P., & Cranmer, S. R. 1995, ApJ, 442, 296
Habing, H., Tignon, J., & Tielens, A. 1994, A&A, 286, 523
Hamann, W.-R., Koesterke, L., & Wessolowski, U. 1993, A&A, 274, 397
Hartmann, L., & MacGregor, K. B. 1982, ApJ, 259, 180
Hester, J. H. et al. 1995, in preparation
Hutsemékers, D., & Van Drom, E. 1991, A&A, 248, 141
Icke, V. 1988, A&A, 202, 177
Iglesias, C. A., & Rogers, F. J. 1991, ApJ, 371, L73
Kahn, F. D., & West, K. A. 1985, MNRAS, 212, 837
Kato, M. 1983, PASJ, 35, 33
Kato, M., & Hachisu, I. 1994, ApJ, 437, 802
Lamers, H. J. G. L. M., Maeder, A., Schmutz, W., & Cassinelli, J. P. 1991, ApJ, 368, 538
Lamers, H. J. G. L. M., & Pauldrach, A. W. A. 1991, A&A, 244, L5
Langer, N., Hamann, W.-R., Lennon, M., Najarro, F., Pauldrach, A. W. A., & Puls, J. 1994, A&A, 290, 819
Leitherer, C., et al. 1994, ApJ, 482, 292
Livio, M. 1994, in Circumstellar Media in Late Stages of Stellar Evolution, ed. R. Clegg, P. Meikle, & I. Stevens (Cambridge: Cambridge Univ. Press), 35
Livio, M., & Soker, N. 1988, ApJ, 329, 764
Lucy, L. B. 1976, ApJ, 205, 482
Lucy, L. B., & Abbott, D. C. 1993, ApJ, 405, 738
Luo, D., & McCray, R. 1991, ApJ, 379, 659
Maheswaran, M., & Cassinelli, J. P. 1994, ApJ, 421, 718
Massa, D., Prinja, R. K., & Fullerton, A. W. 1995, ApJ, 452, 842
Mustel, E. R., & Boyarchyk, A. A. 1970, Ap&SS, 6, 183
Netzer, N., & Elitzur, M. 1993, ApJ, 410, 701
Nota, A., Clampin, M., Sirianni, M., Greenfield, P., & Golimowski, D. A. 1995, in IAU Symp. 163, Wolf-Rayet Stars: Binaries, Colliding Winds, Evolution, ed. K. A. van der Hucht & P. M. Williams (Dordrecht: Kluwer), 78
Nugis, T. 1990, in IAU Symp. 143, Wolf-Rayet Stars and Interrelations with Other Massive Stars in Galaxies, ed. K. A. van der Hucht & B. Hidayat (Dordrecht: Kluwer), 75
O'Dell, C. R., Wen, Z., & Hu, X. 1993, ApJ, 410, 696
Orio, M., Trussoni, E., & Ögelman, H. 1992, A&A, 257, 548
Owocki, S. P., Cranmer, S., & Blondin, J. 1994, ApJ, 424, 887
Paresce, F. 1994, A&A, 282, L13
Poe, C. H. 1987, Ph.D. thesis, Univ. Wisconsin
Poe, C. H., Friend, D. B., & Cassinelli, J. P. 1989, ApJ, 337, 888
Prinja, R. K., Barlow, M. J., & Howarth, I. D. 1990, ApJ, 351, 607
Rosino, L. 1977, Ap&SS, 55, 383
Ruggles, C. L. N., & Bath, G. T. 1979, A&A, 80, 97
Schmutz, W. 1995, A&A, in press
Schulte-Ladbeck, R. E., Clayton, G. C., Hillier, D. J., Harries, T. J., & Howarth, I. D. 1994, ApJ, 429, 846
Schulte-Ladbeck, R. E., Clayton, G. C., Leitherer, C., Drissen, L., Robert, C., Nota, A., & Parker, J. Wm. 1993a, Space Sci. Rev., 66, 193
Schulte-Ladbeck, R. E., Hillier, D. J., & Nordsieck, K. H. 1993b, preprint
Schulte-Ladbeck, R. E., Nordsieck, K. H., Taylor, M., Nook, M. A., Bjorkman, K. S., Magalhães, A. M., & Anderson, C. M. 1991, ApJ, 382, 301
Schulte-Ladbeck, R. E., et al. 1992, ApJ, 401, L105
Sion, E. M., Huang, M., Szkody, P., & Cheng, F. 1995, ApJ, 445, L31
Soker, N. 1994, PASP, 106, 52
Solf, J. 1983, ApJ, 273, 647
Springmann, U. W. E. 1994, A&A, 289, 505
Starrfield, S., Truran, J. W., & Sparks, W. M. 1978, ApJ, 226, 186
Struve, O. 1931, ApJ, 73, 94
van der Hucht, K. A., Cassinelli, J. P., & Williams, P. M. 1986, A&A, 168, 111
Wang, L., & Mazzali, P. A. 1992, Nature, 355, 58
Williams, P. M. 1995, in IAU Symp. 163, Wolf-Rayet Stars: Binaries, Colliding Winds, Evolution, ed. K. A. van der Hucht and P. M. Williams (Dordrecht: Kluwer), 335
Zickgraf, F.-J., Wolf, B., Stahl, O., Leitherer, C., & Appenzeller, I. 1986, A&A, 163, 119
Zickgraf, F.-J., Wolf, B., Stahl, O., Leitherer, C., & Klare, G. 1985, A&A, 143, 421